Field multi-step limestone and MgO passive system to treat acid mine drainage with high metal concentrations

Running title: limestone and MgO passive treatment system

Manuel A. Caraballo[1*], Tobias S. Rötting[2], Francisco Macías[1], José Miguel Nieto[1] and Carlos Ayora[3]

1 Geology Department, University of Huelva, Campus "El Carmen", E-21071 Huelva, Spain

2 Newcastle University, Sir Joseph Swan Institute for Energy Research, Newcastle upon Tyne, NE1 7RU, United Kingdom

3 Institute of Environmental Assessment and Water Research, CSIC, Jordi Girona 18, E-08034 Barcelona, Spain

[*] Corresponding author. Tel.: +34-95-921-9834; fax: +34-95-921-9810

E-mail address: manuel.caraballo@dgeo.uhu.es (Manuel A. Caraballo)

Abstract

Passive treatment systems have become one of the most sustainable and feasible ways of remediating acid mine drainage (AMD). However, conventional treatments present early clogging of the porosity or/and coating of the reactive grains when high acidity and metal concentrations are treated. The performance of fine-grained reagents dispersed in a high porosity matrix of wood shavings was tested as an alternative to overcome these durability problems. The system consisted of two tanks of 3 m^3 filled with limestone sand and wood shavings, and one tank of 1 m^3 with caustic magnesia powder and wood shavings, separated by several oxidation cascades and decantation ponds. The system treated about 1.5 m^3/day of AMD containing an average of 360 mg/L Fe, 120 mg/L Al, 390 mg/L Zn, 10 mg/L Cu, 300 μg/L As and 140 μg/L Pb, a mean pH of 3.08 and a net acidity of 2500 mg/L as $CaCO_3$ equivalents. The water reached pH 5 and 6 in the first and second limestone tanks, respectively (suitable to remove trivalent metals); and pH 8 to 9 in the MgO tank (suitable to remove divalent metals). After nine months of operation, the system achieved an average removal of 100% Al, Cu, As, Pb, more than 70% Fe, about 25% Zn and 80% acidity. Goethite, schwertmannite, hydrobasaluminite, amorphous $Al(OH)_3$ and gypsum were the main precipitates in the two limestone tanks. Precipitation of divalent metals (Fe (II), Zn, and traces of Cd, Ni and Co) were complete inside the third tank of MgO, but preferential flow along the walls was responsible for its low treatment performance. Goethite, gypsum, Zn-schulenbergite and sauconite are the crystalline solid phases identified in the MgO tank.

Keywords

Dispersed Alkaline Substrate, divalent metals removal, passive remediation, Iberian Pyrite Belt

1. Introduction

Polluted mine waters can be remediated by two generic approaches, active or passive treatment (Johnson and Hallberg, 2005). While the former implies the use of energy and continuous addition of chemicals, the later relies on natural water flow and biogeochemical reactions. The Iberian Pyrite Belt (IPB) in the SW of the Iberian Peninsula (Spain) is the largest massive sulfide district in the world with more than one hundred abandoned sites discharging acid mine drainage (AMD) into the Tinto and Odiel rivers (Sánchez-España et al., 2005). The large number of sources and the lack of any current responsible for the pollution suggest passive treatment systems as the most feasible remediation option for the region.

One of the biggest hurdles that a passive treatment system has to overcome is the long operating time necessary to make the system economically feasible (PIRAMID-Consortium, 2003). Clogging of the porosity and coating of the reactive grains with precipitates (passivation) are the two main operating factors controlling the life time of a passive treatment, and both of them depend on the amount of dissolved contaminants in the AMD. Due to the very high metal concentrations of the AMD from the Iberian Pyrite Belt (IPB) (Cánovas et al., 2007; Nieto et al., 2007), the traditional systems like anoxic limestone drains, ALD (Benner et al., 1999; Cocos et al., 2002; Watten et al., 2005) or reducing and alkalinity producing systems, RAPS (Jage et al., 2001), experience clogging or passivation within a few months of operation. A novel reactive material called dispersed alkaline substrate (DAS) was developed to overcome these problems (Rötting et al., 2008a, b). On the one hand, this reactive mixture contains an

65 inert pine wood shavings matrix, to supply a high porosity and to reduce the problems
66 of clogging, and on the other hand, a fine-grained reagent (e.g. limestone) to increase
67 reactivity and to dissolve the reactive grains completely before passivation occurs.
68 Limestone-DAS has been successfully tested in a one year laboratory column study
69 (Rotting et al., 2008a), where the chemical and hydraulic performance were
70 investigated. A complementary field experience in the IPB was also performed showing
71 very promising results (Rötting et al., 2008b). During the operation time, this passive
72 treatment system removed 90-100% Al, Cu, Pb and As, about 45% Fe and an average
73 net acidity of 900 mg/L as $CaCO_3$ equivalents. The important amount of unreacted
74 limestone observed in the reactive tank when it was sampled showed the need for a new
75 study to optimize the limestone-wood shavings ratio of the filling. Moreover, with the
76 exception of Cu, the system did not remove divalent metals (Fe(II), Zn, Cd, Co, Ni, etc).
77 The use of two different alkaline reagents lies in the need to reach pH values between
78 8 and 9, which is impossible to achieve in AMD by limestone dissolution because, due
79 to the high Ca concentration in these waters, equilibrium with this mineral is reached
80 when the pH is between 6 and 7. Magnesium oxide (MgO) dissolution buffers solutions
81 between pH of 8.5 and 10.5, which is high enough to precipitate divalent metals like Zn,
82 Cd, Ni or Co.
83 Laboratory experiments to remove divalent metals with MgO (caustic magnesia) have
84 given promising results. Cortina et al., 2003, treated monometallic synthetic solutions
85 (Zn, Cu, Pb, Mn) of pH between 3 and 5.5 with columns filled with caustic magnesia
86 and quartz sand (2-4 mm grain size). Rötting et al., 2006, repeated the same experiment
87 with Cd, Ni and Co. In all cases metal removal finished after 1,000 to 2,000 pore
88 volumes (less than three months), when the columns clogged, and only a minor fraction
89 of the reactive material was consumed. Some experiments performed with

multicomponent acid input solutions (Al, Fe and some divalent metals) resulted in a much poorer performance (200 pore volumes) due to fast development of Fe-Al coating of the MgO reagent (Cortina et al., 2003). In order to improve the hydraulic conductivity and the consumption of the reactive substrate, a third laboratory column experiment (Rötting et al., 2008c) was performed using a mixture of pine wood shavings, caustic magnesia sand (MgO-DAS) and a synthetic aqueous solution of pH 5.5 with Zn and Mn. During its one year of operation, the experiment completely removed the metals without any clogging.

The present work is the continuation of these experiments, and the objective is to test the performance of a complete limestone and MgO-DAS remediation pilot plant using natural high metal concentration-AMD. The previous pilot plant experiment (Rötting et al., 2008b) was extended to complete the current treatment (Fig. 1), comprising the following elements: one tank of limestone-DAS designed to remove Al, As, and part of Fe, two oxidation cascades and decantation ponds, a second tank of limestone-DAS designed to increase pH to values above 5 and to completely remove Al and Fe(III); finally, and again after oxidation cascades and decantation ponds, a reactive tank of MgO-DAS designed to remove divalent metals. The system was monitored during nine months (when the natural flow of AMD ceased due to a period of drought), and the solids were sampled upon the completion of the treatment in order to characterize solid precipitates.

2. Materials and methods

2.1. Field site and treatment system description

The present study was carried out at the Monte Romero abandoned mine complex put in operation in 1967 by Asturiana de Zinc to obtain Pb and Zn (Pinedo-Vara, 1963),

115 being located near Cueva de la Mora village, in Almonaster la Real, SW of Spain (Fig.
116 1). The ore, mined by underground operations, consists of a massive pyrite deposit with
117 minor amounts of Zn, Pb and Cu sulfides, belonging to the Vulcano-Sedimentary
118 Complex of the IPB (Pinedo-Vara, 1963). The enclosing rocks are low grade phyllites
119 without any carbonate beds.

120 As occurred in many other mines, its closure implied the flooding of the underground
121 galleries due to the end of the groundwater pumping and the generation of AMD. The
122 inflow AMD of the treatment was taken from the emerging water of a mine shaft. The
123 metal concentration and physico-chemical parameters of the AMD (Table 1) reflect the
124 mine mineralogy (Fe, Zn, Cu and Pb sulfides) as well as the almost anoxic conditions
125 (e.g. low Eh and very low dissolved oxygen).

126 A schematic view of the passive treatment system is shown in Fig. 1. The treatment is
127 subdivided in three different sections: two of them consisting of limestone-DAS tanks
128 of 3 m^3 in volume connected in series with two decantation ponds (T1-D1-D2 and T2-
129 D3-D4) and a third section consisting of an MgO-DAS tank of 0.5 m^3 in volume (T3).
130 Each tank was equipped with lateral sampling ports at different depths in order to
131 measure the profiles of chemical parameters. The different elements of the treatment are
132 connected using open, plastic channels and cascades to oxygenate the AMD and
133 promote iron oxidation. On the basis of previous studies (Rötting et al., 2008b), the
134 limestone proportion in T1 was reduced in order to avoid clogging by a massive
135 precipitation of Al. Detailed characteristics of the different elements of the treatment are
136 exposed in Table 2. An inflow rate of 1.5 m^3/day was set to obtain a residence time of at
137 least 24 h for T1 and T2. This flow rate implies a residence time close to 10 h for T3
138 and 4 days for each decantation pond.

Global operating time for the treatment was almost 9 months (from 28 of July 2006 to 1 of April 2007) and the treatment was stopped due to the ceasing of the water supply in the shaft after a very long dry period. The tanks were put into operation sequentially, in order to test that each section was working properly.

2.2. Water sampling and analysis

Water samples were taken at least once a month for the following points: inflowing water, supernatant and drain pipe for T1, T2 and T3 and inflowing and out-flowing water at D1, D2, D3 and D4. Sampling of the lateral ports of each tank was done every other month. Temperature and electrical conductivity were measured in the field using a portable CM35 meter (Crison®) with 3 point calibration (147 and 1413 μS/cm and 12.88 mS/cm). The pH and redox potential were measured using a PH25 meter (Crison®) with Crison electrodes. Redox potential and pH were controlled and calibrated using 2 points (240-470 mV) and 3 points (pH 4.01- 7.00-9.21) respectively, with Crison standard solutions. The redox potential measurements were corrected to the Standard Hydrogen Electrode to calculate pE. Dissolved oxygen was measured with an auto-calibrating Hanna® portable meter and gross alkalinity was determined using CHEMetrics® Total Titrets® (range 10-100 or 100-1000 mg/L as CaCO3 equivalents, accuracy approximately 5%). Water samples were filtered immediately after collection through 0.1 μm Millipore filters on Millipore syringe filter holders, acidified in the field to pH <1 with HNO3 suprapur and stored at 4°C in 60 ml sterile polypropylene containers until analyzed. Analyses were carried out in the Central Research Services of the University of Huelva. Dissolved concentrations of Al, As, Be, Ca, Cd, Co, Cr, Cu, Fe, K, Mg, Mn, Na, Ni, Pb, S, Si, Ti, V and Zn were determined by Inductively Coupled Plasma Atomic Emission Spectrometry (ICP-AES Yobin-Ybon Ultima2) using a

protocol specially designed for AMD samples (Tyler et al., 2004). The detection limit was always lower than 0.1 mg/L, and the analytical error was lower than 5%.

Net acidity (Ac) (mg/L as $CaCO_3$ equivalents) was calculated according to the recommendations from Kirby and Cravotta, 2005a, b, and using the following equation after Rötting et al., 2008b:

$$Ac = 50{,}045 \cdot (3 \cdot c_{Al} + 2 \cdot c_{Fe} + 2 \cdot c_{Mn} + 2 \cdot c_{Zn} + 10^{-pH}) - alk \quad (1)$$

where c_X are molar concentrations of the different metals (mol/L) and alk is measured gross alkalinity (mg/L as CaCO3 equivalents).

Saturation indices (SI = logIAP - logK; IAP = ion activity product) of possible minerals with respect to analyzed element concentrations were calculated using PHREEQC Interactive 2.15.0 (Parkhurst, 1995) and the WATEQ4F database (Ball and Nordstrom, 1991). Additional thermodynamic data for schwertmannite was taken from Yu et al., 1999.

2.3. Solid sampling and analysis

For the solid sampling, 3 cross sections (one for each reactive tank) were dug after the completion of the treatment to have a look at the different precipitate layers developed inside the reactive material. On the basis of the visual study performed at each cross section, the following samples were taken: 0-2, 2-5, 5-10, 10-12, 12-20, 20-40 and 40-90 cm deep for T1; 0-2, 2-5, 5-8, 8-12, 12-18, 18-23, 23-30, 30-40 and 40-60 cm deep for T2 and 0-2, 2-10, 10-20 and 20-40 cm deep for T3.

As a first approach to the constituent mineralogy of the samples, an X-ray diffraction (XRD) study of randomly oriented powder samples was performed using a Bruker D5005 X-ray Diffractometer with Cu Kα radiation. Diffractometer settings were: 40 kV, 30 mA and a scan range of 3–65º 2θ, 0.05º 2θ step size and 20-s counting time per

186 step for the samples with lower crystallinity (iron and zinc precipitates) and 3–65º 2θ,
187 0.02º 2θ step size and 2.4-s counting time per step for the samples with higher
188 crystallinity (samples with gypsum and/or calcite). The low crystallinity of the typical
189 precipitates generated in AMD environments (Dold, 2003; Gagliano et al., 2004; Hall et
190 al., 1996; Kumpulainen et al., 2007; Caraballo et al., 2009a) makes necessary the use of
191 some complementary techniques to consolidate and to extend the first XRD results.
192 Thus, it was decided to perform total digestions and selective mineral dissolutions of the
193 different samples of each reactive tank. Concentrated HNO_3 was employed to achieve
194 the total digestion of the samples while 0.2M NH_4-oxalate was used to differentiate
195 between the Fe corresponding to schwertmannite and to goethite (Dold, 2003). Using
196 the samples submitted to schwertmannite selective dissolution a Differential X-ray
197 Diffraction (DXRD) study was performed (Caraballo et al., 2009a).

198 The metal concentration of the different digestions and selective mineral dissolutions
199 were determined by Inductively Coupled Plasma Atomic Emission Spectrometry (ICP-
200 AES Yobin-Ybon Ultima2).

201

202 **3. Results and discussion**

203 *3.1. Hydrochemistry and mineralogy of the treatment's first section*

204 In order to give an overview of the hydrochemical variation, only three elements (Fe,
205 Al and Zn), pH and alkalinity were selected. As can be observed in Fig. 2, the first
206 important change in the AMD hydrochemistry occurs at the output of T1 (T1-OUT)
207 where pH increases from 3 to almost 5. At the same time, Fe and Al concentrations in
208 the reactive tank decrease from 380 to 326 and from 150 to 50 respectively.

209 The bulk chemistry and mineralogy of the solids present inside T1 is exposed in Fig.
210 3 and table 3, respectively. As can be observed, the upper 10 cm of the reactive
211 material consists of an iron horizon, where only schwertmannite and goethite have been
212 identified by XRD and DXRD. The results obtained from the mineral selective
213 dissolution performed with 0.2M NH_4-oxalate allowed all of the iron to separate into
214 two different sets, one belonging to schwertmannite and the other to goethite. As shown
215 in Figure 3, almost all the iron present in samples at 0-2 and 2-5 cm deep corresponds to
216 iron hosted in schwertmannite while the iron proportion for sample 5-10 cm is close to
217 50% for each mineral. This mineral is poorly represented in XRD because of its low
218 crystallinity. The schwertmannite/goethite ratio decreasing from top to bottom of the
219 iron horizon, is attributed to direct precipitation of schwertmannite from the
220 supersaturated supernatant solution (Table 3) and its aging to goethite with increasing
221 depth. This is the same distribution as previously described in a DAS passive treatment
222 system (Caraballo et al., 2009b) and in terraces naturally formed from the same AMD
223 (Acero et al., 2006).

224 The diffractograms obtained from samples from 10 to 90 cm (Table 3) only reveal the
225 presence of gypsum as a new mineral phase and calcite as part of the initial substrate.
226 Nevertheless, total digestions performed on these samples (Fig. 3) show, as expected, an
227 important aluminum concentration. This difference can be attributed to the presence of
228 amorphous Al-phases. From the Al/S ratio, previous studies have proposed the presence
229 of amorphous basaluminite as fresh precipitates in treatment systems (Rötting et al.,
230 2008b), and as a result of mixing waters in rivers of the region (Sanchez-España et al.,
231 2006). However, molar ratio of aluminum to sulfur for basaluminite is 4 while this
232 value for T1 ranges from 8 to 12. This higher ratio can be explained by the presence of
233 an additional Al-phase, probably amorphous $Al(OH)_3$ (Table 4). Previous studies have

234 also shown the coexistence of basaluminite and gibbsite (Nordstrom, 1982), which are
235 an aging product of other metastable Al-phases (Berkowitz et al., 2006; Berkowitz et
236 al., 2005; Nordstrom, 1982; Sims and Ellis, 1983).

237 The chemical profile of the pore water from T1 (Fig. 4A) shows how iron
238 precipitation is limited to the upper part of the reactive material (first 2 or 3cm deep)
239 and how all the As present in the water is removed coupled to this iron precipitation via
240 adsorption and coprecipitation onto the Fe precipitates. Al water concentration within
241 T1 (Fig. 4A) confirms the hypothesis of Al precipitation when the pH of the AMD
242 reaches a value of more than 5. At the same time and coupled with Al removal some
243 other elements (Cu, Pb and Cr) are completely or almost completely removed inside T1.
244 The removal distribution of all these elements inside the Al precipitation zone suggests
245 that the mineral phases responsible for the Al removal are also responsible for the
246 removal of Cu, Pb and Cr. These observations are in agreement with the study
247 performed to the Fe and Al precipitates formed in the passive treatment system of
248 Monte Romero 2005-2006 (Caraballo et al., 2009b). This study revealed that although
249 some As, Cu, Pb, Zn and Cr were released after the specific sequential extraction step
250 designed to obtain the adsorbed elements, the great majority of these elements were
251 released only after the complete dissolution of the Fe and Al precipitates. As expected
252 from their low concentration, no other solid phases of these minor elements have been
253 detected by XRD. Between 0 and 20 cm, Al, Cu and Pb concentration reach values
254 higher than in the supernatant AMD (Fig. 4A). This is attributed to the redissolution of
255 the Al solid phase caused by the advance of the more acid Fe front. Then, due to the
256 scarcity of calcite reactive surface, part of the alkalinity needed for the Fe minerals to
257 precipitate is supplied by the dissolving Al solid. Regarding Zn, Cd, Co and Ni, Fig. 4A
258 shows that the concentration of these elements remains constant throughout T1.

As shown in Fig. 4B, Al removal efficiency of T1 decreases with time. The most plausible explanation for the time evolution of these three sets of profiles is that gypsum and Al-solid precipitation on limestone surface decreases the reactivity of the latter mineral, which is also shown by lower pH and dissolved Ca. Because Al precipitation only takes place at a pH higher than 5, the decrease in pH with time forces the Al precipitation front to move down into the reactive material. The important Al migration inside T1 and the decrease of the removal efficiency of the reactive material with respect to time, are due to both the lower limestone proportion used in this experiment, compared with previous studies (Rötting et al., 2008a), and the great increase of Al concentration in the AMD (from 70 to 140 mg/L) which occurred halfway through the operation time.

The next important step in the first section of the treatment is the removal of Fe that takes place inside the first decantation pond (Fig. 2, D1-OUT). Part of the remaining Fe(II) is oxidized at the cascades, and additional schwertmannite precipitates from the supersaturated AMD in the decantation pond. The removal of OH^- causes the coupled decrease of pH (Fig. 2). The low pH does not allow metastable Al-phases to precipitate. Amorphous $Al(OH)_3$ is subsaturated (Table 4), and no thermodynamic data for amorphous basaluminite have been found.

3.2. Hydrochemistry and mineralogy of the treatment's second section

The first step of the treatment's second section consists of another limestone-DAS tank (T2) where pH and alkalinity are increased while Fe and Al water concentrations are decreased according to the different reactions previously discussed for T1 (Fig. 2, T2-OUT).

The inspection of the diffractograms and total digestions performed in T2 (Table 3 and Fig. 3) shows small differences between the solid chemistry and mineralogy profile

284 of this tank and the one observed in T1. The iron horizon in T2 (from 0 to 12 cm) is
285 comprised only by goethite as iron mineral phase that agrees with the SI obtained for
286 goethite and schwertmannite in this level (Table 4). The important presence of calcite
287 and gypsum in this layer suggests that goethite precipitation is linked to the dissolution
288 of calcite that increases pH and enhances Fe(II) oxidation. This is different from the
289 situation observed in T1, where schwertmannite precipitated from the supernatant
290 solution. Because of the lower water aluminum concentration in this tank, the aluminum
291 horizon developed inside the reactive material is restricted from 12 to 30 cm. Another
292 important difference between T2 and T1 is that calcite dissolution and gypsum
293 precipitation only took place in the upper 30 cm of the reactive material, leaving 60 cm
294 of unreacted material. Therefore, the durability of tank T2 is double that of T1, or
295 alternatively, one T2 tank can treat the water from two T1 tanks.

296 The distribution of pore water concentrations throughout the profile of T2 is similar
297 to the one described for T1 with the only difference being that the metals removed in T2
298 directly depend on the removal efficiency of T1. Thus, as can be observed in the
299 October-2006 chemical profile of T2 (Fig. 5A), during the time that all the Al present in
300 the T1 water was removed, the only major element removed from inside T2 was Fe,
301 while a very slight Cd, Co and Ni removal can also be observed. Due to the pH of
302 almost 7 achieved during the first months of operation of T2, and the lack of specific
303 precipitates for these minor elements inside T2 (Table 3), this uptake is attributed to the
304 adsorption processes onto goethite. When Al removal in T1 was less efficient, the
305 remaining Al in the water was almost totally removed inside T2 (Fig. 5B, February-
306 2007). As discussed for T1, Cu and Pb are fixed by adsorption and coprecipitation with
307 the Al precipitates (Fig. 5B). Two stages are observed in the chemical profile evolution
308 in T2 (Fig. 5A and B). In the beginning of the experiment (October-2006), Fe removal

309 took place only in the upper 5 cm of the reactive material, while later (February-2007),
310 Fe was removed in the upper 60 cm. Moreover, the pH value at the output of T2
311 decreased from 6.7 in October 2006 to 6.1 in February 2007 (Fig. 5B). No Cd, Co or Ni
312 removal was observed for the lower pH.

313 As described for D1, the same process of schwertmannite precipitation, involving Fe
314 and alkalinity removal and a decrease in pH can be observed in the D3 and D4
315 decantation ponds (Fig. 2, D3-OUT, D4-OUT). Due to the higher pH and alkalinity at
316 the output of T2, the Fe precipitation took place not only in one decantation pond but in
317 both D3 and D4.

318 *3.3. Hydrochemistry and mineralogy of the treatment's third section*

319 The last section of the treatment implies the flow of AMD throughout the MgO-DAS
320 reactive material of T3. At this point, a significant Fe and Zn removal and pH increase
321 can be observed (Fig. 2, T3-OUT). The chemical composition of the precipitates
322 developed inside T3 (Fig. 3) reveals two differentiated layers, a first one from 0 to 2 cm
323 deep with iron as its main constituent, and a second layer from 2 to 40 cm deep mainly
324 composed of zinc. According to the XRD of the sample from 0-2 cm (Table 3), the
325 mineral responsible for Fe removal is goethite. Concerning the mineralogy of the zinc
326 precipitates (Appendix), the most plausible mineral phases are Zn-dominant
327 schulenbergite, $(Zn,Cu,)_7(SO_4)_2(OH)_{10}\bullet 3H_2O$, and sauconite,
328 $Zn_3(Si,Al)_4O_{10}(OH)_2\bullet 4H_2O$. Taking into account the amount of Si and Zn removed from
329 the T3 tank (Table 4), the latter mineral must be a very minor phase. No sign of
330 $Zn(OH)_2$ found in previous laboratory studies with simpler water chemistry (Rötting et
331 al., 2006, 2008c) have been identified, probably due to the complex solution treated in
332 the present case. As expected from their low concentration in the inflow AMD, no solid
333 phases for trace elements have been detected by XRD. It is also important to take into

account that practically the entire reagent is exhausted at the end of the experiment: no peaks of MgO or brucite are evident in the different diffractograms of T3 and only less than 1 mmol Mg/g solid remains in the solid phase (Fig. 3). Therefore, the durability of the tank T3 is slightly shorter than that of T1 suggesting that a larger volume or a higher reagent concentration is needed to increase T3 operating time.

The inspection of a profile of pore water concentrations through the third reactive tank shows three different patterns (Fig. 6): a first one corresponding to the supernatant water (from -5 to 0 cm), a second one representing the water chemistry inside the MgO-DAS reactive material (from 0 to 40 cm) and finally, a third one showing the water chemistry inside the gravel quartz layer (from 40 to 45 cm). The high metal content of the supernatant (Appendix) was completely removed inside the MgO-DAS reactive material, where the water pH reached a value between 8 and 9. However, all the metals present in the supernatant appear again in the quartz gravel drain with the concentrations of all solutes diluted to a proportion close to 0.6 (Appendix). This suggests that only 0.4 of the water circulated through the reactive material (with the complete removal of metals), while another portion of 0.6 flowed down through preferential paths to the quartz drain where both waters mixed. This matches the development of red channels of iron oxide observed along the semitransparent plastic walls of the tank.

3.4. Removal efficiency of the treatment

According to equation 1, the net acidity can be considered as a very useful parameter to evaluate the efficiency of each section of the treatment regarding metal removal and water hydrochemistry improvement. Time evolution of the net acidity at four selected points of the treatment as well as Fe, Al and Zn concentration are shown in Fig. 7. The

359 inflow net acidity suffered a sudden increase three months after the beginning of the
360 experiment. This increase was due to a very important rise of the concentrations of Fe,
361 Al and Zn (Appendix and Fig. 7).

362 The net acidity removal (INFLOW net acidity – D2-OUT net acidity) of the first
363 section of the treatment (T1+D1+D2) ranges from 500 mg/L as $CaCO_3$ equivalent,
364 during the first three months, to almost 1,000 mg/L after the sudden increase of net
365 acidity in December. It decreases to almost 700 mg/L towards the end of the experiment
366 (Appendix). The decrease of the net acidity in this section of the treatment is clearly
367 linked to the Fe removal in T1 and D1 and, in a higher proportion, to the Al removal
368 inside T1, and its average is similar to the 900 mg/L reported by Rötting et al., 2008b,
369 for an equivalent tank with 20% v/v of limestone. Examination of the net acidity
370 removal in the second section of the treatment (T2+D3+D4) reveals a mean removal of
371 around 500 mg/L as $CaCO_3$ equivalent and Fe being the main element removed. Finally,
372 the net acidity removal at the outflow of the treatment (T3-OUT) shows a decrease of
373 another 500 mg/L as $CaCO_3$ equivalent. This final decrease is due to the Zn and Fe
374 removal inside T3. All in all, the system is able to decrease the net acidity from 2,500 to
375 500 mg/L as $CaCO_3$ equivalents.

376 In order to evaluate the global removal efficiency, the mean relative metal removal of
377 the system was calculated according to the following equation:

$$r = \frac{c_{in} - c_{out}}{c_{in}} \cdot 100 \qquad (2)$$

378

379 where c_{in} corresponds to the system inflow concentration of a certain element and c_{out} to
380 the system outflow concentration of the same element. The results of these calculations
381 are presented in Fig. 8, where the inflow and outflow mean concentration and the mean

382 relative removal for some elements have been grouped in two different graphics (Fig.
383 8A and B) corresponding to major and minor elements. Concerning the major elements
384 (Fig. 8A), a relative removal close to 100% for Al and Cu, higher than 70% for Fe and
385 Si and almost 25% for Zn can be observed. These relative removals imply a mean net
386 removal from the inflow water after the treatment of: 300 mg/L Fe, 140 mg/L Al, 105
387 mg/L Zn, 32 mg/L Si and 12 mg/L Cu. In the case of minor elements (Fig. 8B), a
388 relative removal of 100% for As and Pb, higher than 95% for Cr, almost 20% for Ni, 10
389 % for Co and 5% for Cd can be observed. These relative removals imply a mean net
390 removal from the inflow water of: 460 μg/L As, 155 μg/L Pb, 220 μg/L Ni, 95 μg/L
391 Co, 70 μg/L Cd and 14 μg/L Cr.

392

393 **4. Conclusions**

394 Summarizing some of the most relevant observations defining the treatment efficiency,
395 the system is able to remove a net acidity around 2,000 mg/L as $CaCO_3$ equivalents
396 leading to a decrease in the inflow of AMD from 2,500 to 500 mg/L as $CaCO_3$
397 equivalents. This acidity removal is double that achieved with only one limestone-DAS
398 tank (Rötting et al., 2008b) and much higher than the removal rates achieved by anoxic
399 limestone drains, RAPS and similar passive systems (theoretical alkalinity generation
400 up to 350-450 mg/L as $CaCO_3$; Younger et al., 2002; average field values of 240-290
401 mg/L, respectively, Ziemkiewicz et al., 2003). Net acidity elimination corresponds to a
402 relative removal close to 100% for Al and Cu, higher than 70% for Fe and almost 25%
403 for Zn (regarding major elements) and 100% for As and Pb, and higher than 95% for
404 Cr.

405 Although the optimal proportion of limestone sand in the limestone-DAS reactive
406 material depends on the AMD hydrochemistry, the present study has shown that a
407 12.5% (v/v) shows similar removal to 20%(v/v) limestone (Rötting et al., 2008b).
408 However, a decrease in reactivity is observed at the end of our experiment. This is
409 attributed to the faster progress of the aluminum precipitation front down through the
410 reactive material, which causes a lower removal of Al inside T1, less increase in
411 alkalinity and less iron removal in the subsequent decantation ponds. The second
412 limestone-DAS tank (T2) and the following two decantation ponds, play an important
413 role in Fe removal (almost 50% of the whole removal of the system). Both Fe and Al
414 removal are important to ensure an efficient and long performance of MgO treatment
415 (Cortina et al., 2003). Analysis of T3 revealed that almost all the reactive material
416 present in this MgO-DAS tank was consumed. This observation clearly shows that the
417 chosen grain size was suitable to achieve a total dissolution before any passivation
418 process appeared. However, higher volume and/or higher MgO proportion in the
419 reactive material are needed to extend T3 operating time. The T3 tank confirms that
420 MgO is able to remove completely divalent metals such as Zn, Fe(II), Cd, Co and Ni
421 from a complex aqueous solution extending the results of previous laboratory
422 experiments. However, T3 shows a clear problem of preferential flow along the walls.
423 To avoid this problem, T3 should be similar to T1 and T2 (with no evident preferential
424 flow), i.e., with higher volume, cylindrical shape and made of fiberglass. Mina
425 Esperanza passive treatment system (Almonaster la Real, Spain) can be cited in order to
426 have a look at an up-scaled limestone-DAS tank to treat the whole outflow of an adit at
427 the Iberian Pyrite Belt (Caraballo et al., 2008). This system used 300 m^3 of limestone-
428 DAS to treat a maximum flow of 1L/s during an operating time of 18 months.

The mineralogy of the precipitates developed in the passive treatment system is directly linked to the precipitation of the five main elements present in Monte Romero AMD: Fe, Al, Ca, Zn and SO_4. Accordingly, an iron horizon was precipitated at the top of the reactive material of T1, T2 and T3. This iron layer was comprised by schwertmannite and goethite in T1 and only by goethite (with minor amounts of gypsum) in T2 and T3. Schwertmannite seems to precipitate directly from the supersaturated supernatant water, and ages progressively to goethite similar to the process observed in the terraces of the same AMD flow. Goethite precipitates within the upper pores of the treatment, where limestone or MgO dissolves, and the subsequent rise in pH accelerates the Fe(II) oxidation. Next, an aluminum horizon forms inside T1 and T2. No crystalline Al phase could be detected at this layer, amorphous $Al(OH)_3$ and basaluminite being the most plausible aluminum phases. Finally, only a zinc horizon was present inside T3. Unlike $Zn(OH)_2$ found in previous laboratory experiments, complex minerals such as Zn-dominant schulenbergite, $(Cu,Zn)_7(SO_4)_2(OH)_{10}•3H_2O$, and minor sauconite, $Zn_3(Si,Al)_4O_{10}(OH)_2•4H_2O$ are proposed as the most probable Zn-rich precipitates.

Acknowledgments

We gratefully acknowledge Mari Paz Martín, Rafael Carrasco and María José Ruíz (Central Research Services of the University of Huelva) for assistance in XRD and chemical analysis. This study was funded by the Spanish Government projects CTM2006-28151-E/TECNO and CTM2007-66724-/TECNO. M.A.C. was financially supported by the Spanish Government with a FPU PhD fellowship. We also like to thank Anne Thompson and David Vaughan (Associate editors) and two anonymous reviewers for their comments that significantly improved the quality of this paper.

454

455 **References**

456 Acero, P., Ayora, C., Torrentó, C., Nieto, J.M., 2006. The behavior of trace elements
457 during schwertmannite precipitation and subsequent transformation into goethite
458 and jarosite. Geochim. Cosmochim. Acta 70, 4130-4139.

459 Ball, J.W., Nordstrom, D.K., 1991. User's manual for WATEQ4F with revised
460 thermodynamic database and test cases for calculating speciation of major, trace
461 and redox elements in natural waters. US Geol. Surv. Water-Resour. Investig.
462 Rep. 91–183.

463 Benner, S.G., Blowes, D.W., Gould, W.D., Herbert, R.B., Ptacek, C.J., 1999.
464 Geochemistry of a permeable reactive barrier for metals and acid mine drainage.
465 Environ. Sci. Technol. 33, 2793-2799.

466 Berkowitz, J., Anderson, M.A., Amrhein, C., 2006. Influence of aging on phosphorus
467 sorption to alum floc in lake water. Water Res. 40, 911-916.

468 Berkowitz, J., Anderson, M.A., Graham, R.C., 2005. Laboratory investigation of
469 aluminum solubility and solid-phase properties following alum treatment of lake
470 waters. Water Res. 39, 3918-3928.

471 Cánovas, C.R., Olías, M., Nieto, J.M., Sarmiento, A.M., Cerón, J.C., 2007.
472 Hydrogeochemical characteristics of the Tinto and Odiel Rivers (SW Spain).
473 Factors controlling metal contents. Sci. Total Environ. 373, 363-382.

474 Caraballo, M.A., Macías, F., Rötting, T.S., Nieto, J.M., Ayora, C., 2008. Disperse
475 Alkaline Substrate passive remediation at Mina Esperanza (Iberian Pyrite Belt,
476 SW Spain). Geochimica et Cosmochimica Acta 72, A135.

477 Caraballo, M.A., Rotting, T.S., Nieto, J.M., Ayora, C., 2009a. Sequential extraction and
478 DXRD applicability to poorly crystalline Fe- and Al-phase characterization from
479 an acid mine water passive remediation system. Am. Min. 94, 1029-1038.
480 Caraballo, M.A., Nieto, J.M., Ayora, C., 2009b. Iron and aluminum precipitates as
481 metals and metalloids sinks in a passive treatment system. Geochim.
482 Cosmochim. Acta 73, A191.
483 Cocos, I.A., Zagury, G.J., Clément, B., Samson, R., 2002. Multiple factor design for
484 reactive mixture selection for use in reactive walls in mine drainage treatment.
485 Water Res. 36, 167-177.
486 Cortina, J.L., Lagreca, I., De Pablo, J., Cama, J., Ayora, C., 2003. Passive in situ
487 remediation of metal-polluted water with caustic magnesia: evidence from
488 column experiments. Environ. Sci. Technol. 37, 1971-1977.
489 Dold, B., 2003. Speciation of the most soluble phases in a sequential extraction
490 procedure adapted for geochemical studies of copper sulfide mine waste. J.
491 Geochem. Explor. 80, 55-68.
492 Gagliano, W.B., Brill, M.R., Bigham, J.M., Jones, F.S., Traina, S.J., 2004. Chemistry
493 and mineralogy of ochreous sediments in a constructed mine drainage wetland.
494 Geochim. Cosmochim. Acta 68, 2119-2128.
495 Hall, G.E.M., Vaive, J.E., Beer, R., Hoashi, M., 1996. Selective leaches revisited, with
496 emphasis on the amorphous Fe oxyhydroxide phase extraction. J. Geochem.
497 Explor. 56, 59-78.
498 Jage, C.R., Zipper, C.E., Noble, R., 2001. Factors affecting alkalinity aeneration by
499 successive alkalinity-producing systems: regression analysis. J. Environ. Qual.
500 30, 1015-1022.

501 Johnson, D.B., Hallberg, K.B., 2005. Acid mine drainage remediation options: a review.
502 Sci. Total Environ. 338, 3-14.
503 Kirby, C.S., Cravotta, C.A., 2005a. Net alkalinity and net acidity 1: Theoretical
504 considerations. Appl. Geochem. 20, 1920-1940.
505 Kirby, C.S., Cravotta, C.A., 2005b. Net alkalinity and net acidity 2: Practical
506 considerations. Appl. Geochem. 20, 1941-1964.
507 Kumpulainen, S., Carlson, L., Räisänen, M.L., 2007. Seasonal variations of ochreous
508 precipitates in mine effluents in Finland. Appl. Geochem. 22, 760-777.
509 Nieto, J.M., Sarmiento, A.M., Olías, M., Cánovas, C.R., Riba, I., Kalman, J., Delvalls,
510 T.A., 2007. Acid mine drainage pollution in the Tinto and Odiel rivers (Iberian
511 Pyrite Belt, SW Spain) and bioavailability of the transported metals to the
512 Huelva Estuary. Environ. Internat. 33, 445-455.
513 Nordstrom, D.K., 1982. The effect of sulfate on aluminum concentrations in natural
514 waters: some stability relations in the system Al2O3-SO3-H2O at 298 K.
515 Geochim. Cosmochim. Acta 46, 681-692.
516 Pinedo-Vara, I., 1963. Piritas de Huelva. Su historia, minería y aprovechamiento.
517 Summa, Madrid, Spain.
518 Parkhurst, D.L., 1995. User's guide to PHREEQC: a computer program for speciation,
519 reaction path, advective-transport, and inverse geochemical calculations. US
520 Geol. Surv. Water-Resour. Investig. Rep. 95–4227.
521 PIRAMID-Consortium, 2003. Engineering guidelines for the passive remediation of
522 acidic and/or metalliferous mine drainage and similar wastewaters. European
523 Commission Fifth Framework RTD Project No. EVK1-CT-1999-000021
524 ''Passive In-situ Remediation of Acidic Mine/Industrial Drainage" (PIRAMID).
525 University of Newcastle, Newcastle Upon Tyne, UK.

526 Rotting, T.S., Cama, J., Ayora, C., Cortina, J.L., DePablo, J., 2006. Use of caustic
527 magnesia to remove cadmium, nickel, and cobalt from water in passive
528 treatment systems: column experiments. Environ. Sci. Technol. 40, 6438-6443.
529 Rötting, T.S., Thomas, R.C., Ayora, C., Carrera, J., 2008a. Passive treatment of acid
530 mine drainage with high metal concentrations using dispersed alkaline substrate.
531 J. Environ. Qual. 37, 1741-175.
532 Rötting, T.S., Caraballo, M.A., Serrano, J.A., Ayora, C., Carrera, J., 2008b. Field
533 application of calcite Dispersed Alkaline Substrate (calcite-DAS) for passive
534 treatment of acid mine drainage with high Al and metal concentrations. Appl.
535 Geochem. 23, 1660-1674.1.
536 Rötting, T.S., Ayora, C., Carrera, J., 2008c. Improved passive treatment of high Zn and
537 Mn concentrations using Caustic Magnesia (MgO): Particle size effects.
538 Environ. Sci. Tech. 24, 9370–9377.
539 Sánchez-España, J., Pamo, E., Pastor, E., Andrés, J., Rubí, J., 2005. The natural
540 attenuation of two acidic effluents in Tharsis and La Zarza-Perrunal mines
541 (Iberian Pyrite Belt, Huelva, Spain). Environ. Geol. 49, 253-266.
542 Sánchez-España, J., Pamo, E., Pastor, E., Andrés, J., Rubí, J., 2006. The removal of
543 dissolved metals by hydroxysulphate precipitates during oxidation and
544 neutralization of acid mine waters, Iberian Pyrite Belt. Aquatic Geochem. 12,
545 269-298.
546 Sims, J.T., Ellis, B.G., 1983. Changes in phosphorous sorption associated with aging of
547 aluminum hydroxide suspensions. Soil Sci. Soc. Am. J. 47, 912-916.
548 Tyler, G., Carrasco, R., Nieto, J.M., Pérez, R., Ruiz, M.J., Sarmiento, A.M., 2004.
549 Optimization of major and trace element determination in acid mine drainage

samples by ultrasonic nebulizer-ICP-OES (USN-ICP-OES). Pittcon 2004 Conference, Chicago, USA.

Watten, B.J., Sibrell, P.L., Schwartz, M.F., 2005. Acid neutralization within limestone sand reactors receiving coal mine drainage. Environ. Pollut. 137, 295-304.

Yu, J.Y., Heo, B., Choi, I.K., Cho, J.P., Chang, H.W., 1999. Apparent solubilities of schwertmannite and ferrihydrite in natural stream waters polluted by mine drainage. Geochim. Cosmochim. Acta 63, 3407-3416.

Ziemkiewicz, P.F., Skousen, J.G., Simmons, J., 2003. Long-term performance of passive acid mine drainage treatment systems. Mine Water Environ. 22, 118–129.

FIGURE CAPTIONS

Fig. 1. Field site location and schematic view of the different sections comprising Monte Romero DAS passive treatment system. T1 and T2 correspond to limestone DAS-tanks, T3 is the MgO DAS-tank and D1-4 are the four decantation ponds. AMD flows from T1 to T3.

Fig. 2. Fe (mg/L), Al (mg/L), Zn (mg/L), pH and alkalinity (mg/L as $CaCO_3$ equivalents) distribution at some representative points of the passive treatment system in February 2007. Legend: Tn-IN = Tank n inflow, Tn-Sup = Tank n supernatant, Tn-OUT = Tank n outflow, Dn-OUT = Decantation pond n outflow.

Fig. 3. Bulk chemistry of some representative samples of the solid profile sampled at the three reactive tanks. Fe (Sch) = iron hosted in schwertmannite, Fe (Gth) = iron hosted in goethite.

Fig. 4. (A) Chemical profile of the first limestone-DAS reactive tank in October 2006. The values at -5 cm of depth represent the supernatant. (B) Time evolution of pH, precipitated aluminium and dissolved calcium in the first limestone-DAS reactive tank.

Fig. 5. Chemical profile of the second limestone-DAS reactive tank in October 2006 (A) and February 2007 (B). The values at -5 cm of depth represent the supernatant.

Fig. 6. Chemical profile of the MgO-DAS reactive tank in February 2006. The values at -5 cm of depth represent the supernatant.

Fig. 7. Time evolution of the net acidity, Fe, Al, and Zn concentration at some strategic points of the passive treatment system. D2 and D4 correspond to decantation ponds 2 and 4 respectively and T3 corresponds to the MgO reactive tank.

Fig. 8. Metal concentration at the system inflow and outflow and relative removal of the whole system for some major (A) and minor (B) elements. The values shown in this graph correspond to the last three months of the system when all the reactive tanks were in operation.

FIG. 1.

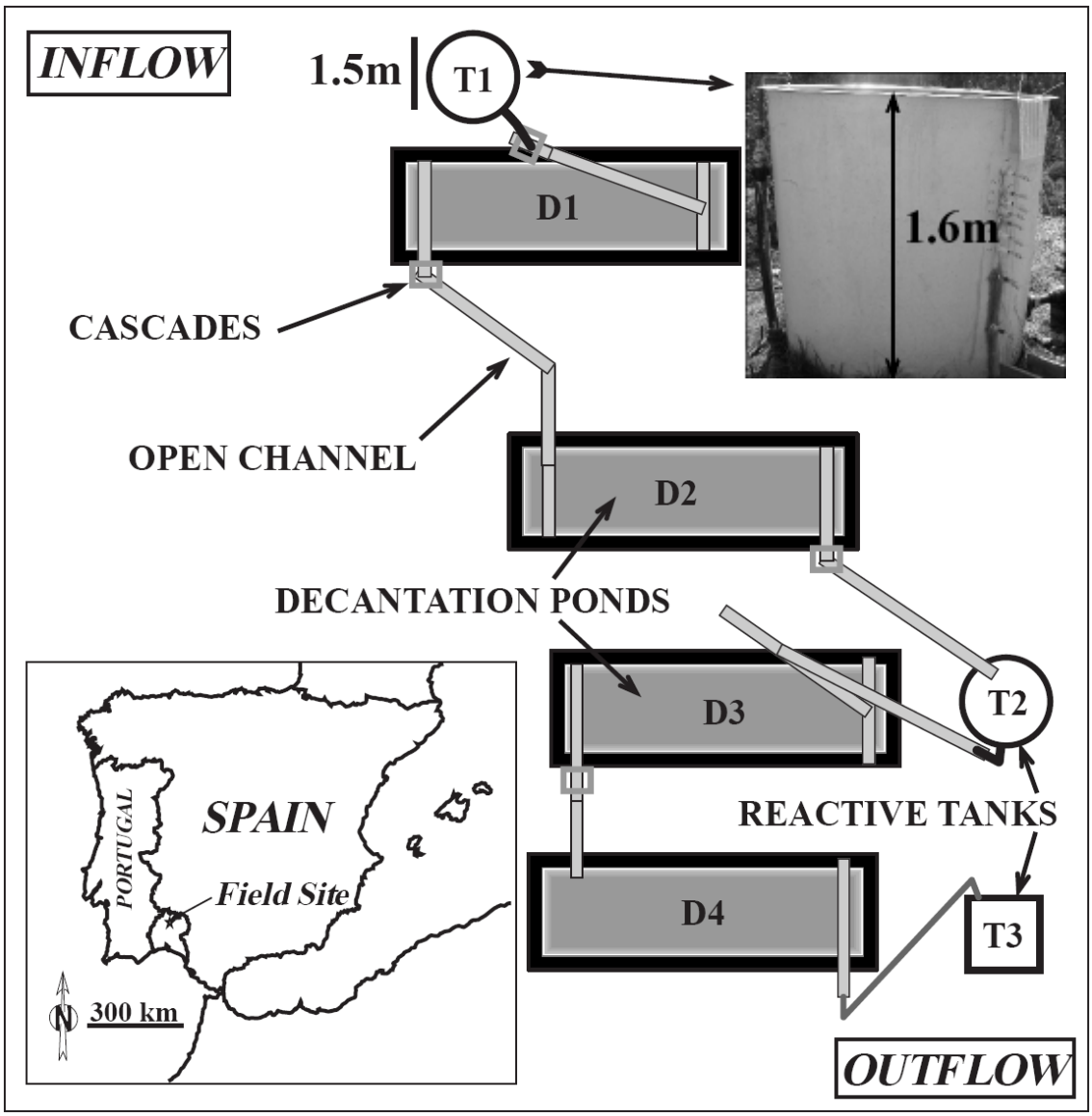
INFLOW
1.5m
T1
D1
1.6m
CASCADES
OPEN CHANNEL
D2
DECANTATION PONDS
D3
T2
REACTIVE TANKS
D4
T3
OUTFLOW
SPAIN
PORTUGAL
Field Site
300 km

FIG. 2.

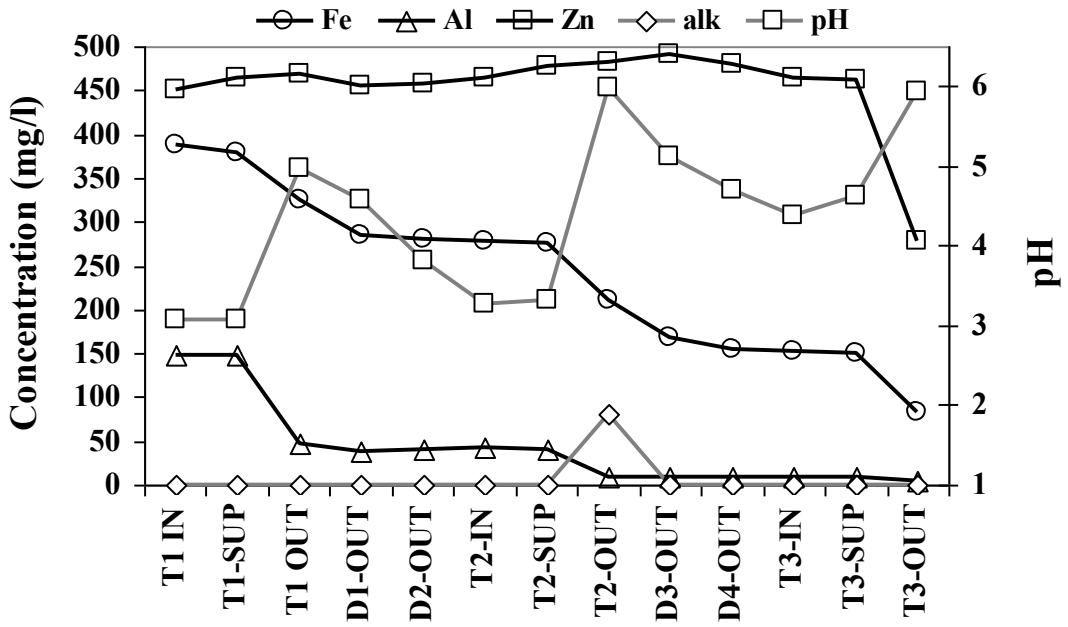
Fe
Al
Zn
alk
pH
Concentration (mg/l)
500
450
400
350
300
250
200
150
100
50
0
6
5
4
3
2
1
pH
T1 IN
T1-SUP
T1 OUT
D1-OUT
D2-OUT
T2-IN
T2-SUP
T2-OUT
D3-OUT
D4-OUT
T3-IN
T3-SUP
T3-OUT

FIG. 3.

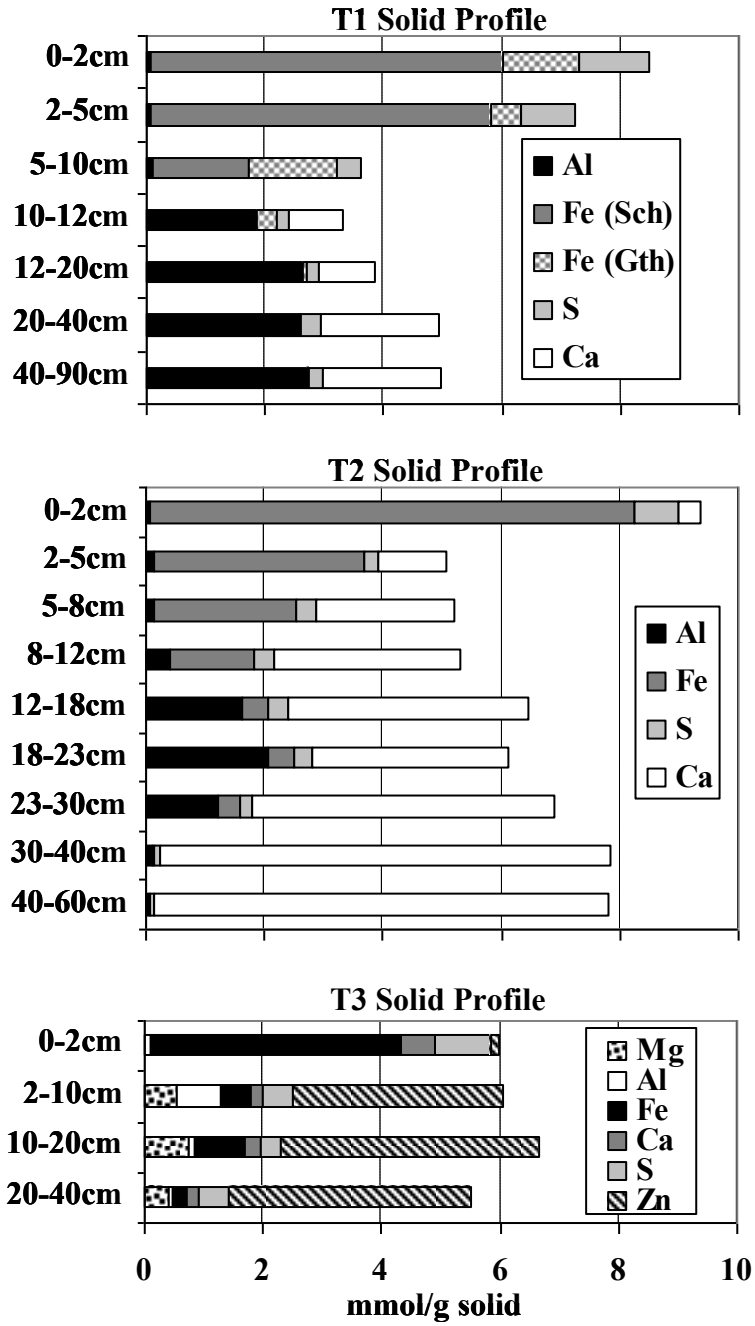
T1 Solid Profile
0-2cm
2-5cm
5-10cm
10-12cm
12-20cm
20-40cm
40-90cm
Al
Fe (Sch)
Fe (Gth)
S
Ca
T2 Solid Profile
0-2cm
2-5cm
5-8cm
8-12cm
12-18cm
18-23cm
23-30cm
30-40cm
40-60cm
Al
Fe
S
Ca
T3 Solid Profile
0-2cm
2-10cm
10-20cm
20-40cm
Mg
Al
Fe
Ca
S
Zn
0
2
4
6
8
10
mmol/g solid

FIG. 4.

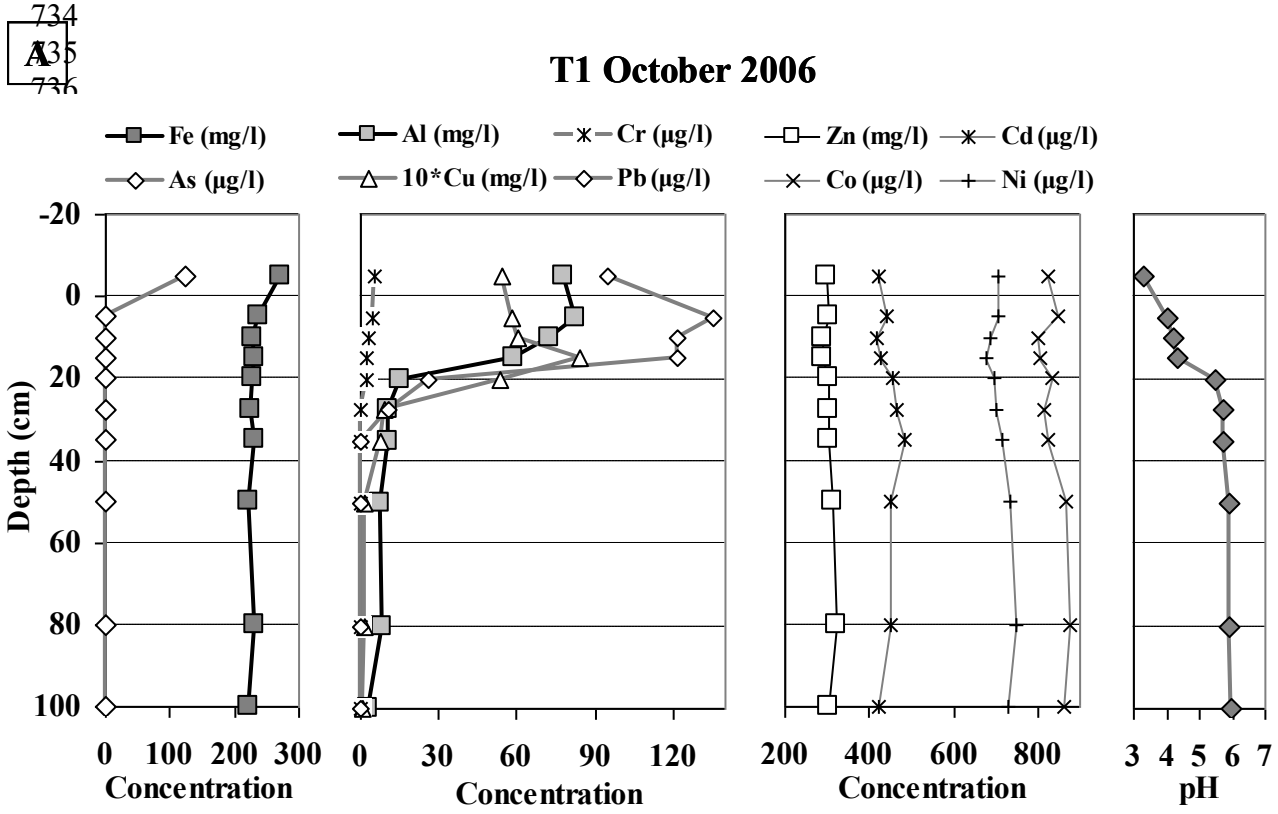
A
T1 October 2006
Fe (mg/l)
Al (mg/l)
Cr (µg/l)
Zn (mg/l)
Cd (µg/l)
As (µg/l)
10*Cu (mg/l)
Pb (µg/l)
Co (µg/l)
Ni (µg/l)
Depth (cm)
-20
0
20
40
60
80
100
0 100 200 300
Concentration
0 30 60 90 120
Concentration
200 400 600 800
Concentration
3 4 5 6 7
pH

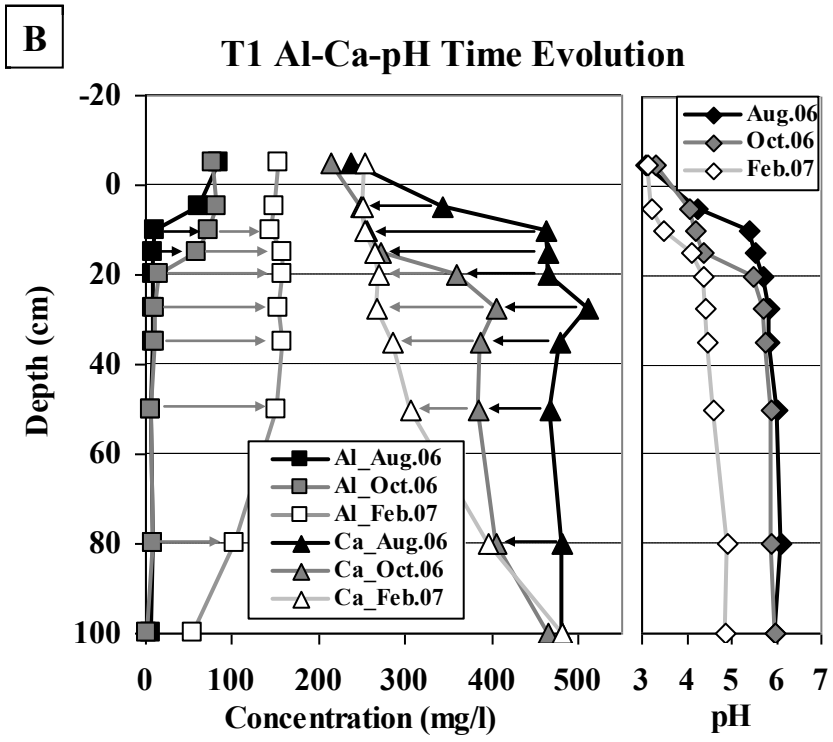
B
T1 Al-Ca-pH Time Evolution
Depth (cm)
-20
0
20
40
60
80
100
Al_Aug.06
Al_Oct.06
Al_Feb.07
Ca_Aug.06
Ca_Oct.06
Ca_Feb.07
Aug.06
Oct.06
Feb.07
0 100 200 300 400 500
Concentration (mg/l)
3 4 5 6 7
pH

FIG. 5.

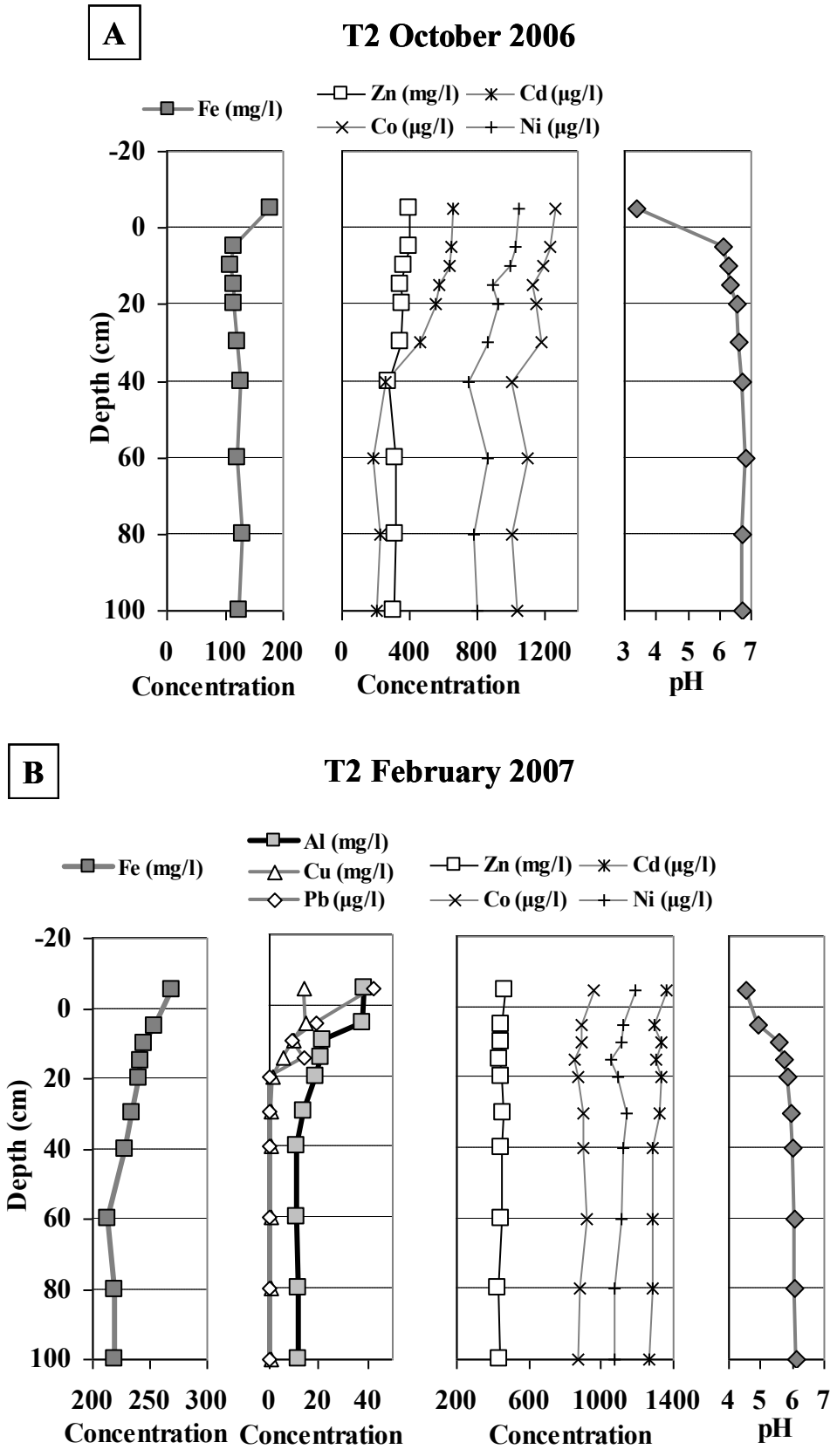
A
T2 October 2006
Fe (mg/l)
Zn (mg/l)
Cd (µg/l)
Co (µg/l)
Ni (µg/l)
-20
0
20
40
60
80
100
Depth (cm)
0 100 200
Concentration
0 400 800 1200
Concentration
3 4 5 6 7
pH
B
T2 February 2007
Fe (mg/l)
Al (mg/l)
Cu (mg/l)
Pb (µg/l)
Zn (mg/l)
Cd (µg/l)
Co (µg/l)
Ni (µg/l)
-20
0
20
40
60
80
100
Depth (cm)
200 250 300
Concentration
0 20 40
Concentration
200 600 1000 1400
Concentration
4 5 6 7
pH

FIG. 6.

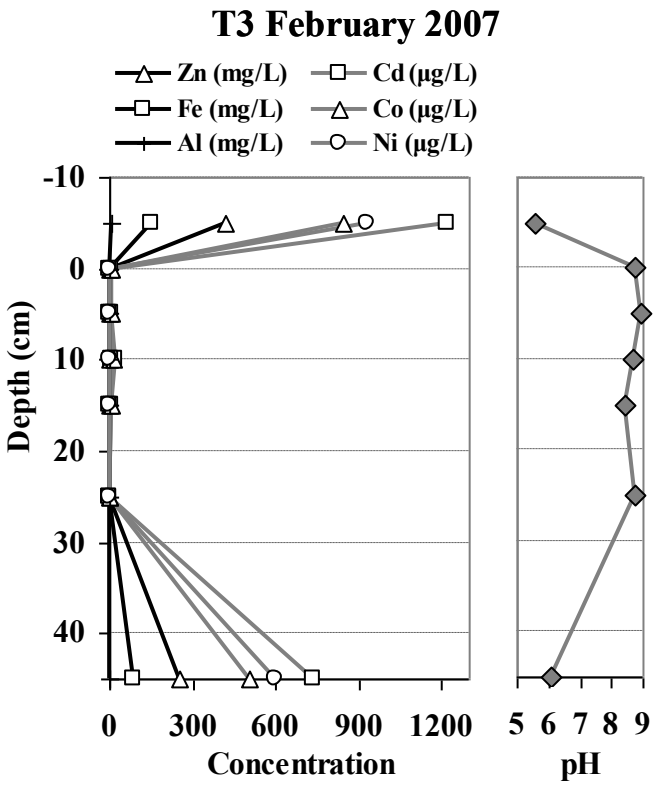
T3 February 2007
Zn (mg/L)
Cd (µg/L)
Fe (mg/L)
Co (µg/L)
Al (mg/L)
Ni (µg/L)
Depth (cm)
-10
0
10
20
30
40
0
300
600
900
1200
Concentration
5
6
7
8
9
pH

FIG. 7.

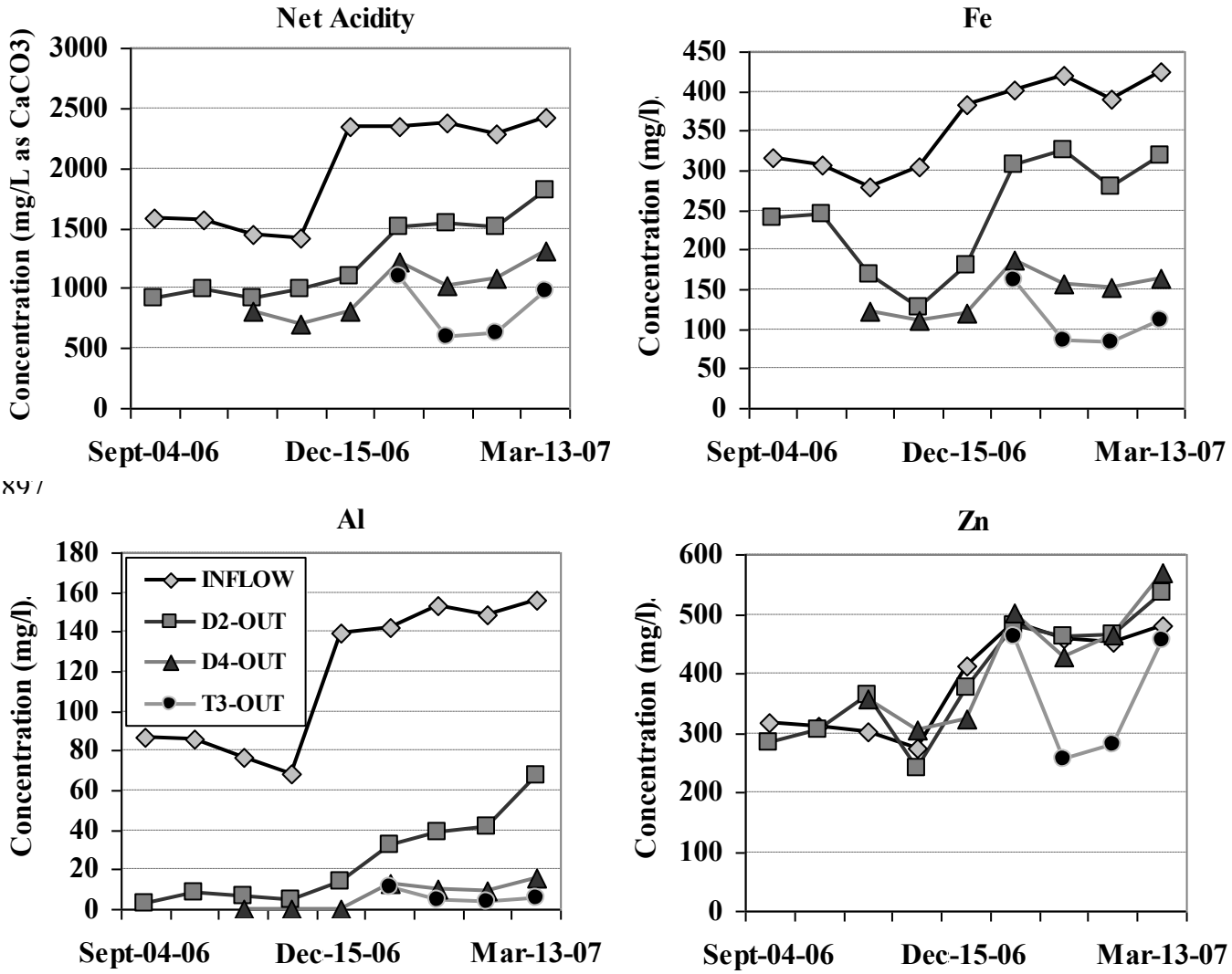
Net Acidity
Concentration (mg/L as CaCO3)
3000
2500
2000
1500
1000
500
0
Sept-04-06
Dec-15-06
Mar-13-07
Fe
Concentration (mg/l)
450
400
350
300
250
200
150
100
50
0
Sept-04-06
Dec-15-06
Mar-13-07
Al
Concentration (mg/l)
180
160
140
120
100
80
60
40
20
0
INFLOW
D2-OUT
D4-OUT
T3-OUT
Sept-04-06
Dec-15-06
Mar-13-07
Zn
Concentration (mg/l)
600
500
400
300
200
100
0
Sept-04-06
Dec-15-06
Mar-13-07

FIG. 8.

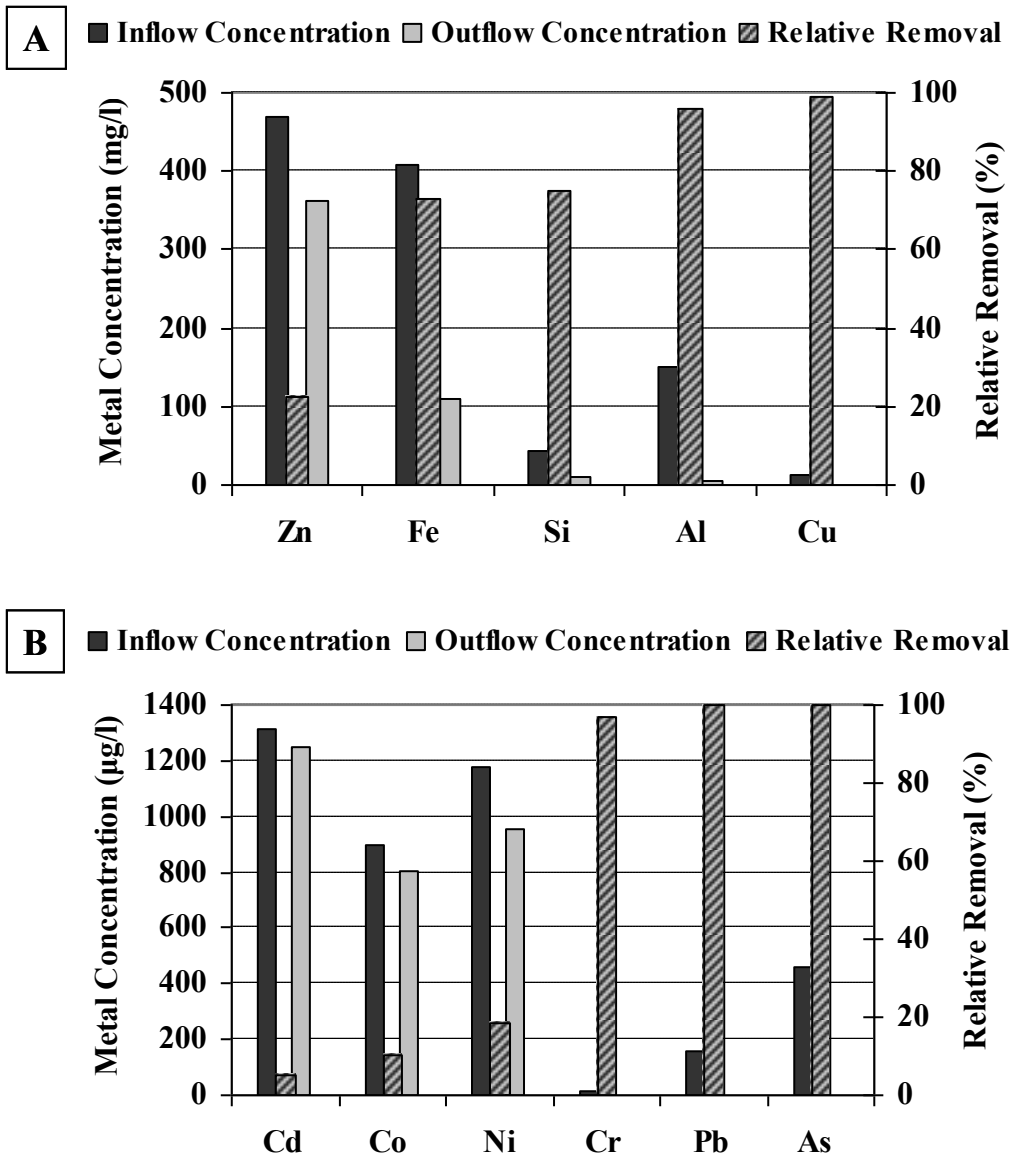
A
Inflow Concentration
Outflow Concentration
Relative Removal
Metal Concentration (mg/l)
Relative Removal (%)
500
400
300
200
100
0
100
80
60
40
20
0
Zn
Fe
Si
Al
Cu
B
Inflow Concentration
Outflow Concentration
Relative Removal
Metal Concentration (µg/l)
Relative Removal (%)
1400
1200
1000
800
600
400
200
0
100
80
60
40
20
0
Cd
Co
Ni
Cr
Pb
As

973 **TABLES**

974

975

Table 1
Mean inflow metal concentration and physico-chemical parameters

Major Elements (mg/L)									
Al	Ca	Cu	Fe	Mg	Mn	Na	Si	SO_4	Zn
117	239	10	358	267	19	18	41	3640	388
Minor Elements (µg/L)									
As	Be	Cd	Co	Cr	Li	Ni	Pb	Ti	V
302	21	915	910	10	395	973	143	3	14

Physic-chemical Parameters				
pH	Eh	Conductivity	Diss. Oxygen	T (ºC)
3.08	571 (mV)	4.6 (mS/cm)	0.9 (mg/L)	17

976 Calculations were made for 10 samplings from July 28, 2006 and April 1, 2007
977
978
979
980

Table 2
Detailed description of the treatment constituent elements

Name	Constituent element	Reactive material
T1	$3m^3$ cylindrical fiberglass tank, perforated pipe and a 15cm layer of quartz gravel as a drain. Lateral sampling ports at 5, 10, 15, 20, 27, 35, 50 and 80 cm deep in the reactive material	12.5% (v/v) of limestone sand and 87.5% (v/v) of pine wood shavings
T2	$3m^3$ cylindrical fiberglass tank, perforated pipe and a 15cm layer of quartz gravel as a drain. Lateral sampling ports at 5, 10, 15, 20, 30, 40, 60, 80 and 100 cm deep in the reactive material.	20% (v/v) of limestone sand and 80% (v/v) of pine wood shavings
T3	$1m^3$ cubic plastic tank, a 5 cm layer of quartz gravel as a drain. Lateral sampling ports at 0, 5, 10, 15, 25, 45 cm deep in the reactive material.	10% (v/v) of MgO powder and 90% (v/v) of pine wood shavings
D1-4	$6m^3$ decantation ponds, dug in the ground and isolated with UV-proof plastic.	

981
982

983

984

Table 3
Mineral phases confirmed with X-ray Diffraction (XRD) and Differential X-ray Diffraction (DXRD)

T1	Depth Ranges(cm)	Mineral Phases			
		Schwertmannite	Goethite	Gypsum	Calcite
	0-2	DXRD	XRD		
	2-5	DXRD	XRD		
	5-10	DXRD	XRD		
	10-12			XRD	XRD
	12-20			XRD	XRD
	20-40			XRD	XRD
	40-90			XRD	XRD

T2	Depth Ranges(cm)	Mineral Phases		
		Goethite	Gypsum	Calcite
	0-12	XRD	XRD	XRD
	12-18		XRD	XRD
	18-23		XRD	XRD
	23-30		XRD	XRD
	30-40		XRD	XRD
	40-60			XRD

T3	Depth Ranges(cm)	Mineral Phases			
		Goethite	Gypsum	Sauconite	Zn-Sch
	0-2	XRD	XRD		
	20-40			XRD	XRD

To mark the presence of a certain mineral phase at each depth and the used analytical technique, the words XRD and DXRD have been used. Zn-Sch = Zinc dominant Schulenbergite.

Table 4

Saturation index (SI) values for the most probably Al and Fe precipitates calculated at some representative points and times of the treatment using PHREEQC Interactive 2.15.0

October 2006		$Al(OH)_3$	Basal	Gib	Gth	Schw	Gyp
T1	-5 cm	-5.7	-10.7	-3.0	4.3	0.9	-0.4
	5 cm	-2.4	0.3	0.3	5.0	2.5	-0.2
	10 cm	0.3	8.7	3.0	6.4	9.1	-0.1
	15 cm	0.5	9.4	3.2	6.6	10.9	-0.1
	20 cm	0.9	10.6	3.6	6.9	12.7	-0.1
D2-out		-0.8	4.9	1.9	5.1	0.1	-0.1
T2	-5 cm	-5.9	-12.0	-3.2	3.1	-9.2	0.0
February 2007							
T1	-5 cm	-5.3	-9.1	-2.6	4.8	4.8	-0.3
	0 cm	-5.1	-8.4	-2.4	4.9	5.5	-0.3
	5 cm	-4.3	-5.8	-1.6	5.0	5.6	-0.3
	10 cm	-2.3	0.8	0.4	6.0	10.9	-0.3
	15 cm	-1.6	3.1	1.1	6.2	11.6	-0.3
	22.5 cm	-1.5	3.6	1.2	6.2	11.2	-0.3
	30 cm	-1.3	4.3	1.4	6.2	11.3	-0.3
D2-out		-5.5	-10.1	-2.8	4.4	1.3	0.0
T2	-5 cm	-1.8	2.1	0.9	5.9	8.8	0.0
	5 cm	-0.6	6.2	2.1	6.7	13.7	0.0
	10 cm	1.0	11.2	3.7	7.3	15.7	0.0
	15 cm	1.3	12.2	4.0	7.4	16.3	0.0
	20 cm	1.5	12.8	4.2	7.6	17.3	0.1
	30 cm	1.5	12.6	4.2	7.6	17.5	0.1
	40 cm	1.5	12.5	4.2	7.8	18.5	0.1
D4-out		-2.8	-1.7	-0.1	5.5	5.7	0.1
T3	-5 cm	0.7	9.9	3.4	8.1	22.5	0.0

$Al(OH)_3$, $Al(OH)_3$ amorphous; Basal, Basaluminite; Gib, Gibbsite; Gth, Goethite; Sch, Schwertmannite and Gyp, Gypsum.

993